

Variational Inexact Image Matching

Ganesh Swaminathan*
School of Engineering Science
Simon Fraser University, Canada

Supervised by: Dr. Faisal Beg[†]
Medical Image Analysis Lab
School of Engineering Science
Simon Fraser University, Canada

September 10, 2007

Abstract

Image registration is the process by which images acquired by different sensors of different objects at different times are matched. The matching is done via an optimization of a set of spatial transformations. Using the fluid model, the Large Deformation Diffeomorphic Metric Mapping (LDDMM) algorithm allows us to define metrics over the space of anatomical images. The focus of this report is on the development and applications of LDDMM in Computational Anatomy.

*ganesh@iamganesh.com

[†]mfbeg@ensc.sfu.ca

Contents

List of Figures	iv
Nomenclature	v
1 Background	1
1.1 Rigid Transformation	1
1.2 Affine Transformation	2
1.3 Nonrigid Transformation	3
1.4 Diffeomorphism	4
1.5 Well-posedness	4
2 Physical Models	5
2.1 Elastic Matching	5
2.2 Fluid Matching	6
3 Large Diffeomorphic Deformation Metric Mapping	8
3.1 Norms and the operator L	8
3.2 Metrics on \mathcal{T}	9
3.3 Gradient	10
3.4 Momentum	11
4 Applications	12
4.1 Atlas Computation	12
4.2 Statistical Shape Analysis	13

4.3 Hippocampal Shape Discrimination	15
5 Conclusion	18
6 Acknowledgments	19
Glossary	20
Index	23
References	23

List of Figures

1	Rigid Transformation	2
2	Non-rigid Transformation	3
3	Diffeomorphic Transformations and their compositions	4
4	Time indexed deformation field	6
5	Nonrigid registration	7
6	Atlas construction	13
7	Hippocampus	15
8	Eigenvalue distribution	17
9	Empirical \hat{F} distribution	18

Nomenclature

α, γ α ensures smoothness, γ is positive so that the operator is non-singular

$\langle f, g \rangle$ Inner product

\mathbf{u} $\mathbf{u} : \Omega \rightarrow \mathbb{R}^3$, displacement vector fields

\mathbf{v} Instantaneous Velocity

\mathcal{G} $\Omega \rightarrow \Omega$, group of diffeomorphisms on Ω

\mathcal{I} the space of anatomies

\mathcal{P} probability measures on the set of transformations belonging to \mathcal{G}

μ, λ Navier-Lamé constants

∇^2 $\frac{\partial^2}{\partial x^2} + \frac{\partial^2}{\partial y^2} + \frac{\partial^2}{\partial z^2}$

$\|\cdot\|_2$ L^2 -norm

$\|\cdot\|_{L^2}$ L^2 -norm

Ω $\Omega \in \mathbb{R}^3$, template coordinate space

σ Smoothing term

φ the composition $I_0 \circ \varphi \approx I_1$ transforms I_0 to I_1

A^\dagger Adjoint of operator A

I_α Deformable template image under a group of diffeomorphisms \mathcal{G}

V Hilbert space of vector fields

1 Background

Medical Image Analysis has seen tremendous growth in the last few years. Improvements in computing power, scanner performance and storage facilities has led to a dramatic increase in the volume of data to be processed. Traditionally, analysis has been done by expert clinicians manually, but this doesn't scale with the datasets available nowadays.

Patient diagnosis often makes use of information from images that are obtained using different imaging modalities. For example, Magnetic Resonance Imaging (MRI) reveal information about the proton density in a particular region of the body. Positron Emission Tomography (PET) is used to evaluate biological processes by measuring concentrations of positron-emitting radioisotopes in living tissue.

Before any interpretations can be made by the clinician, images need to be aligned so that points in one image can be related to points in another. Images acquired at different time points may also need to be aligned. It is the task of *registration* algorithms to achieve such an alignment. Modern registration algorithms also enable the construction of inter-subject atlases for statistical studies across large population groups.

1.1 Rigid Transformation

Consider the two images I_0 and I_1 in figure 1. The target image I_1 has been rotated and scaled. Our objective is to determine a transformation φ such that

$$I_1 = \varphi \circ I_0$$

where the notation $\varphi \circ I_0$ means that the transformation is applied to image I_0 . In this case, the transformation φ would belong to the group of rigid transformations $SE(n)$, corresponding to all $(n + 1) \times (n + 1)$ orthogonal matrices that allow rotation $SO(n)$ and translation.

$$\left\{ \left(\begin{array}{cc} R & t \\ 0 & 1 \end{array} \right) \middle| R \in SO(n) \text{ and } t \in \mathbb{R}^n \right\}$$

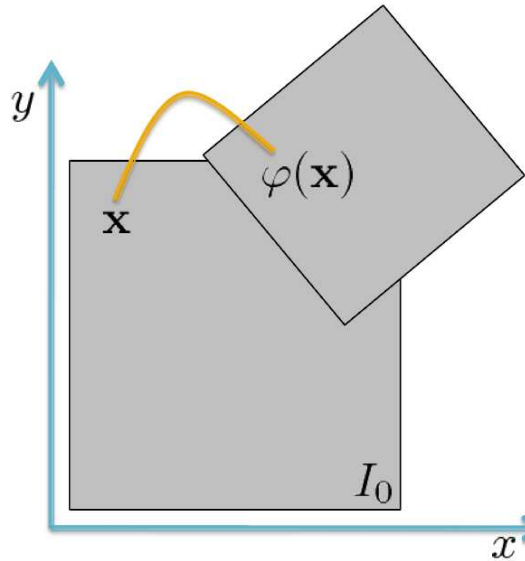


Figure 1: Rigid Transformation

Transformations of this kind are *isometric*, i.e., they preserve angles between lines and distances between points. In 2-dimensions, there are three unknowns and in 3-dimensions, there are six unknowns. The particular example in figure 1 does not have a φ of this kind because it includes scaling.

1.2 Affine Transformation

Affine transformations extend the kind of matrices in section 1.1 to include scaling, shearing and projection. In matrix form,

$$\begin{bmatrix} x' \\ y' \\ z' \end{bmatrix} = \begin{bmatrix} a_{00} & a_{01} & a_{02} \\ a_{10} & a_{11} & a_{12} \\ a_{20} & a_{21} & a_{22} \end{bmatrix} \begin{bmatrix} x \\ y \\ z \end{bmatrix} + \begin{bmatrix} t_x \\ t_y \\ t_z \end{bmatrix}$$

In general, matrix \mathbf{A} is not orthogonal. Affine transformations being linear transformations preserve collinearity between points and ratios of distances along a line.

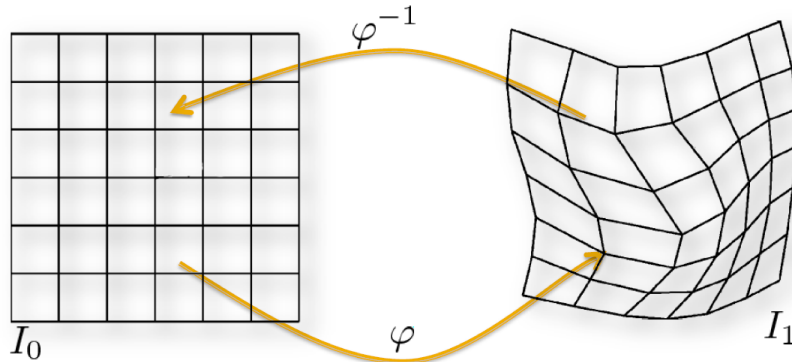


Figure 2: Non-rigid Transformation[6]

1.3 Nonrigid Transformation

Non-rigid transformations allow a wide range of free-form deformations. Transformations of this kind usually have several hundred thousand degrees of freedom, requiring substantially more computing power than rigid or affine transformations. Various models such as spline-based have been proposed, but the most popular are consistent linear elasticity models usually used for small deformations, and models based on viscous fluid models for large deformations.

A grid is defined over the pixels of the source image I_0 as in figure 2. At each grid point, a displacement vector $u(x) : \Omega \rightarrow \mathbb{R}^d$ is calculated to the resulting image I_1 . The transformation function φ and its inverse φ^{-1} are defined as

$$\begin{aligned}\varphi(x) &= x + u(x) \\ \varphi^{-1}(x) &= x - u(x)\end{aligned}$$

The registration problem becomes an optimization problem on the displacement vector field $u(x)$. The norm is taken to be the standard L^2 -norm.

$$\hat{u} = \operatorname{argmin}_u \|\varphi \circ I_0 - I_1\|_{L^2}^2 \quad (1.1)$$

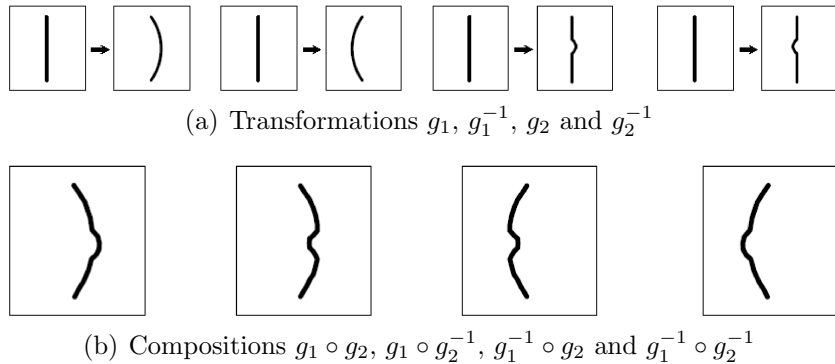


Figure 3: Diffeomorphic Transformations and their compositions[9].

1.4 Diffeomorphism

The transformations defined thus far are ideally well behaved. The group of diffeomorphisms are transformations that are invertible, one-to-one, onto and with continuous differentiable inverses. We denote this group with the notation \mathcal{G} . Transformations of this kind ensure that there is no anatomical tearing or folding, as these do not happen in reality.

Figure 3 demonstrates a set of diffeomorphic transformations. The composition of diffeomorphic transformations in any way also results in a diffeomorphic one. This allows one to derive a more complicated diffeomorphic transformation from a set of simple ones.

1.5 Well-posedness

The optimization problem presented in equation 1.1 is not nicely behaving, or mathematically speaking not well-posed. According to Hadamard[12], a problem is well-posed when a solution to the problem exists, the solution is unique and errors in output depend continuously on errors in input within reasonable topology. Small input errors do not cause large errors in results. As medical images are typically noisy, which inherently is random, we would like to modify the problem statement so that it is well-posed.

One way to fix the ill-posedness of the problem is by including a *regularizer*

term along with the dissimilarity term in the cost functional. The new cost functional now takes the form

$$\hat{u} = \operatorname{argmin}_u \underbrace{\|Lu\|_2^2}_{E1} + \frac{1}{\sigma^2} \underbrace{\|\varphi \circ I_0 - I_1\|_2^2}_{E2} \quad (1.2)$$

The term E1 is the regularizer, restricting the space of solutions to smooth ones with an appropriate constraint. One of the many choices for the regularizer are diffusion, curvature, linear-elasticity or fluid-viscosity. The term E2 is the dissimilarity term and could be one a L^p -norm, cross-correlation, correlation ratio or mutual information. Mutual information specially works very well for cross-modality registration. The σ term is a constant that balances between the dissimilarity and the regularizer terms and allows some leeway for inexact matching.

2 Physical Models

Physical continuum models have been used in computer graphics for many years. In medical imaging analysis, the models were used for regularizing purposes. Some of the first work on nonrigid registration used linear elastic models[2]. The model was based on linearizing the elasticity operator that often broken down for large deformations. Realizing the deficiencies of elastic models, Christensen proposed[7] the viscous fluid model. In the following two sections, the elastic model and the fluid model are described.

2.1 Elastic Matching

Nonrigid registration using elastic continuum models were first proposed by Bajcsy and Kovačič[2]. They modeled the template as a linear elastic solid and deformed it using forces derived from the gradient of a correlation based similarity metric. Miller, Christensen, et al.[17] also used a elastic deformation model, but used a Gaussian sensor model based on a least-squares measure of the grey-level differences between the two images. If

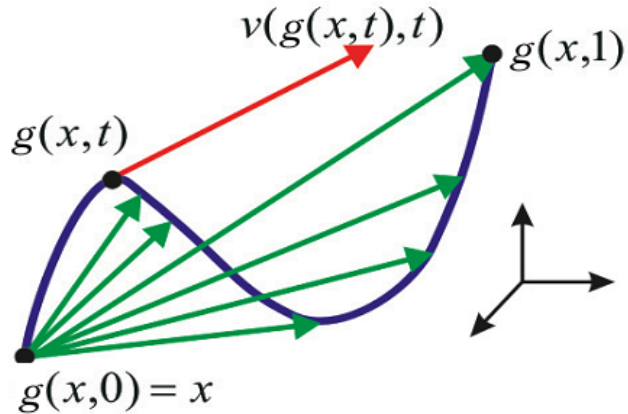


Figure 4: Time indexed deformation field[7]

the images to be registered differ only by Gaussian noise, then the optimal similarity measure is the sum of squared differences as proved by Viola[20].

The deformation is directly modeled using the Navier-Cauchy equilibrium equations for linear elasticity

$$\mu \nabla^2 \mathbf{u} + (\lambda + \mu) \nabla(\nabla \cdot \mathbf{u}) + b(x, \mathbf{u}) = 0$$

where λ and μ are known as Navier-Lamé constants. Engineering textbooks have tables with constants for the elastic properties of different materials. The regularizer term $(\mu \nabla^2 + (\lambda + \mu) \nabla(\nabla \cdot \cdot))$ ensures the smoothness of transformations and will penalize large deformations. Large deformations are necessary for intersubject and atlas-to-subject registration tasks and the elastic model does not guarantee a diffeomorphic deformation for such tasks.

2.2 Fluid Matching

Christensen realized that the small deformation assumption from linearizing the elasticity operator was often violated in intersubject and atlas-to-subject registration. He proposed[7] a viscous fluid model that treats the deformation as a time indexed vector field. This model allows large deformations while maintaining the smoothness.

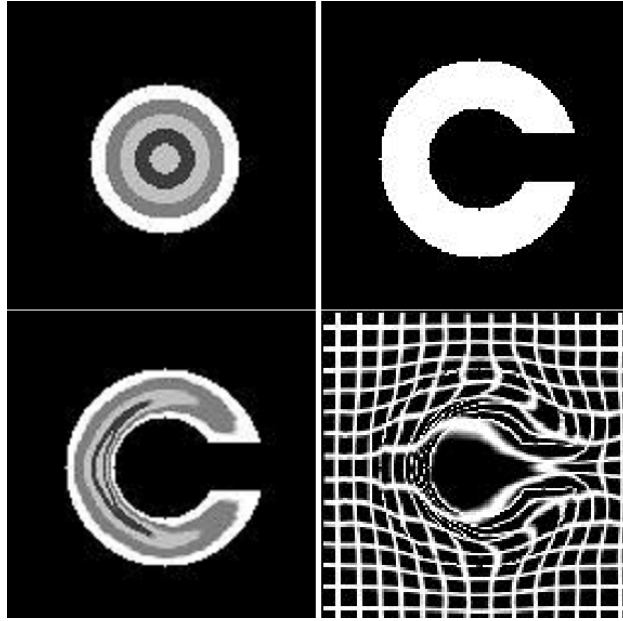


Figure 5: Nonrigid registration of a circle to a 'C'. The top row shows the source and the target images. The bottom right image shows the final registered image. The bottom left image shows the deformation field.

A time indexed deformation field $\mathbf{u}(x, t)$ is generated from the instantaneous velocity $\mathbf{v}(t)$ in the model by the integration of a simple ordinary differential equation

$$\mu \nabla^2 \mathbf{v} + (\lambda + \mu) \nabla (\nabla \cdot \mathbf{v}) + b(x, \mathbf{u}) = 0$$

$$\frac{d\mathbf{u}}{dt} = \mathbf{v}(t, \mathbf{u}(t))$$

where λ and μ are viscosity constants, \mathbf{v} is the instantaneous velocity, \mathbf{b} is the body force per unit volume acting on the body based on a Gaussian sensor model. The equations were solved by Successive Over Relaxation[3].

3 Large Diffeomorphic Deformation Metric Mapping

Christensen, Rabbitt and Miller[7] proposed the large deformation model for computing transformations that overcomes the limitations of small deformations. Large Deformation Diffeomorphic Metric Mapping (LDDMM) is similar to Christensen’s algorithm in the sense that it provides a setting for large deformations by ensuring that transformations are diffeomorphic. Additionally, the length of the shortest path $\inf \int_0^1 \|v(t)\|_V dt$ defines a metric between images I_0 and I_1 . The path generated by Christensen’s algorithm is only locally optimal and thus is not a metric on the image orbit \mathcal{I} .

As in Christensen’s algorithm, the transformations generated by LDDMM are diffeomorphic (see section 1.4). These are of considerable interest in medical imaging as under these transformations, connected sets remain connected, disjoint sets remain disjoint, smoothness of curves, surface and other features are preserved. Thus, there is no change in the anatomical topology.

$$\hat{v} = \operatorname{argmin}_v \left(\int_0^1 \|v(t)\|_V^2 dt + \frac{1}{\sigma^2} \|I_0 \circ \varphi - I_1\|_{L^2}^2 \right) \quad (3.1)$$

$$\begin{aligned} \frac{d\phi(t)}{dt} &= v(t, \phi(t)) \\ \varphi &= \phi(0) + \int_0^1 v(t, \phi(t)) dt \end{aligned}$$

The transformation φ is generated by the optimizing velocity vector field \hat{v} of equation 3.1. The norm $\|\cdot\|_V$ on the velocity ensures sufficient smoothness, and thus in the space of diffeomorphisms.

3.1 Norms and the operator L

The norm of a vector space is determined by the choice of inner product

$$\|x\| = \sqrt{\langle x, x \rangle}$$

The smoothness on the velocity vector field is ensured by a differential operator $L : V \rightarrow L^2(\Omega, \mathbb{R}^d)$ such that

$$\langle f, g \rangle_V = \langle Lf, Lg \rangle_{L^2} \quad (3.2)$$

$$= \langle L^\dagger Lf, g \rangle_{L^2} \quad (3.3)$$

The details of the construction of L are described in [11]. In LDDMM, L is of the Navier-Cauchy type

$$L = (-\alpha \nabla^2 + \gamma) I_{m \times n}$$

Constants α and $\gamma > 0$ are required to enforce smoothness and to make the operator non-singular. When periodic boundary conditions are assumed, L becomes self-adjoint. From L , a unique compact self-adjoint operator $K : L^2(\Omega, \mathbb{R}^d) \rightarrow V$ is defined as

$$K = (L^\dagger L)^{-1} \quad (3.4)$$

such that following equations 3.2 and 3.3

$$\langle f, g \rangle_{L^2} = \langle Kf, g \rangle_V$$

Another advantage of picking the form of operator L is its linear nature. Linear operators are diagonal in the Fourier basis and thus the use of the Fourier basis for evaluating $f = (L^\dagger L)^{-1}g$ is efficient via the Fast Fourier Transform (FFT).

3.2 Metrics on \mathcal{I}

If $\varphi_0, \varphi_1 \in \mathcal{G}$ are two points, the curve $\phi(t, v) \in \mathcal{G}$, $t \in [0, 1]$ from the optimizing velocity \hat{v} in equation 3.1, then the equation given by

$$\rho_{\mathcal{G}}(\varphi_0, \varphi_1) = \int_0^1 \|v(t)\|_V dt$$

is the distance between them. φ_0 and φ_1 are the endpoints $\phi(t, v)|_{t=0}$ and $\phi(t, v)|_{t=1}$. This distance is a true metric as it is positive, symmetric and satisfies the triangle inequality property[5].

A metric on the anatomical ensemble \mathcal{I} is defined by

$$\rho_{\mathcal{I}}(I_0, I_1) = \inf\{\rho_{\mathcal{G}}(Id, \varphi) \mid I_1 = I_0 \circ \varphi, \varphi \in \mathcal{G}\}$$

Moreover, as the curve $\varphi(t)$ is a geodesic, it satisfies the Euler-Lagrange equations. It is also interesting to note that the same curve $\varphi(t)$ makes the kinetic energy functional of the fluid

$$E[v] = \frac{1}{2} \int_0^1 \|v(t)\|_V^2 dt$$

stationary, i.e., the critical points of the two functionals are the same. This can be proved by deriving the Euler-Lagrange equations for the two functionals and showing that they are the same.

3.3 Gradient

The Fréchet derivative $\nabla_v E_t$ in space V is

$$(\nabla_v E_t)_V = 2\hat{v}_t - K \left(\frac{2}{\sigma^2} |D\phi_{t,1}^{\hat{v}}| \nabla J_t^0 (J_t^0 - J_t^1) \right) \quad (3.5)$$

where $J_t^0 = \phi_{t,0} I_0$ and $J_t^1 = \phi_{t,1} I_1$, $|Dg|$ is the determinant of the Jacobian matrix and K is a compact self-adjoint operator $K : L^2(\Omega, \mathbb{R}^3) \rightarrow V$, as defined in equation 3.4, section 3.1. This is referred to as the Hilbert Gradient and is computed according to the inner product on V .

If we were to write the gradient $\nabla_v E_t$ in space V and in space $L^2(\Omega, \mathbb{R}^n)$

$$\begin{aligned} (\nabla_v E_t)_V &= 2v_t + K b_t \\ (\nabla_v E_t)_{L^2} &= 2(L^\dagger L)v_t + b_t \end{aligned}$$

where $b_t = \frac{-2}{\sigma^2} |D\phi_{t,1}^v| \nabla J_t^0 (J_t^0 - J_t^1)$. The advantage of using K over $L^\dagger L$ is clearer when we expand the two operators in an orthonormal basis $(w_i)_{i \in \mathbb{N}}$. The expressions for $(\nabla_v E_t)_{L^2}$ and $(\nabla_v E_t)_V$ becomes

$$\begin{aligned} (\nabla_v E_t)_{L^2} &= \sum_{i \in \mathbb{N}} (\langle 2(L^\dagger L)v_t, w_i \rangle_{L^2} + \langle b_t, w_i \rangle_{L^2}) w_i \\ &= \sum_{i \in \mathbb{N}} (\lambda_i \langle 2v_t, w_i \rangle_{L^2} + \langle b_t, w_i \rangle_{L^2}) w_i \end{aligned}$$

$$\begin{aligned}
(\nabla_v E_t)_V &= \sum_{i \in \mathbb{N}} (\langle 2v_t, w_i \rangle_{L^2} + \langle K b_t, w_i \rangle_{L^2}) w_i \\
&= \sum_{i \in \mathbb{N}} (\langle 2v_t, w_i \rangle_{L^2} + \langle b_t, K^\dagger w_i \rangle_{L^2}) w_i \\
&= \sum_{i \in \mathbb{N}} \left(\langle 2v_t, w_i \rangle_{L^2} + \frac{\langle b_t, w_i \rangle_{L^2}}{\lambda_i} \right) w_i
\end{aligned}$$

using the fact that the operator K is self-adjoint ($K = K^\dagger$). According to a mathematical property[16], if operator \mathcal{A} has eigenvalues λ_i , then \mathcal{A}^{-1} has eigenvalues $1/\lambda_i$. Operator K is also compactly supported, therefore as $i \rightarrow \infty$, the eigenvalues $1/\lambda_i \rightarrow 0$ while $\lambda_i \rightarrow \infty$. This means that the use of the L^2 gradient amplifies high frequency components, while the V gradient smoothens these components as seen by the multiplication and division of the basis coefficients by the eigenvalues. Thus, the use of the V gradient is more stable numerically.

The V gradient is used in a standard steepest descent scheme

$$v^{n+1} = v^n - \epsilon \nabla_{v^n} E$$

The constraints on space V result in good convergence and stability.

3.4 Momentum

LDDMM makes the orbit of the deformable template into a metric space with a metric between elements through geodesic diffeomorphic curves. Deriving the Euler-Lagrange equations from the variational equations 3.1 gives the optimal flow between such elements. This setting has several similarities with the mechanics of perfect fluids, for which the Euler-Lagrange equations have been derived by Arnold[1] for the group of divergence free volume preserving diffeomorphisms.

Recently, a link was established between momentum conservation and geodesic evolution equations[18]. The implications of this link are profound. Once the optimizing velocity field \hat{v} is computed, the entire flow can be parameterized by a single point in time at $t = 0$. Given the velocity $v_t|_{t=0}$, or as later defined the momentum $(L^\dagger L)v_t|_{t=0}$, the entire flow can be regenerated, known as *geodesic shooting*.

The Fréchet derivative in 3.5 of the variational cost 3.1 vanishes on the optimizing flow, i.e., $\nabla_v E_t = 0$. Rearranging equation 3.5

$$\begin{aligned} 2\hat{v}_t &= K \left(\frac{2}{\sigma^2} |D\phi_{t,1}^{\hat{\phi}}| \nabla J_t^0(J_t^0 - J_t^1) \right) \\ (L^\dagger L)v_t &= \left(\frac{1}{\sigma^2} |D\phi_{t,1}^{\hat{\phi}}| \nabla J_t^0(J_t^0 - J_t^1) \right) \end{aligned}$$

According to the rigorous construction of geodesic shooting presented in [18], the quantity $(L^\dagger L)v_t$ is the momentum of the flow at time $t \in [0, 1]$. At time $t = 0$,

$$(L^\dagger L)v_0 = \frac{1}{\sigma^2} |D\phi_{0,1}| [I_0 - I_1 \circ \phi_{0,1}] \nabla I_0$$

and the partial differential equation for the conservation of momentum is

$$(L^\dagger L)v_t = |D\phi_{t,0}| (D\phi_{t,0})^t (L^\dagger L)v_0 \circ \phi_{t,0}$$

The “information-compressing” scheme of the Euler equations additionally provides a linear setting for the entire nonlinear diffeomorphic shape space, enabling one to use the usual linear statistics to do shape analysis.

4 Applications

4.1 Atlas Computation

Computing the average, a single representative image of an anatomical object for a large human population is an important research objective in Computational Anatomy (CA). Atlases are used for pathology detection, algorithm guidance for knowledge-based image analysis, automated structure extraction, image labeling and functional image analysis[19].

Image intensities or transformations cannot be simply averaged as these do not form a vector space. Linear averaging does not respect the “curved manifold” that these images lie in. Linear averaging can be used in a small deformation setting with good results, but cross-population images show immense variability that lead to large deformations.

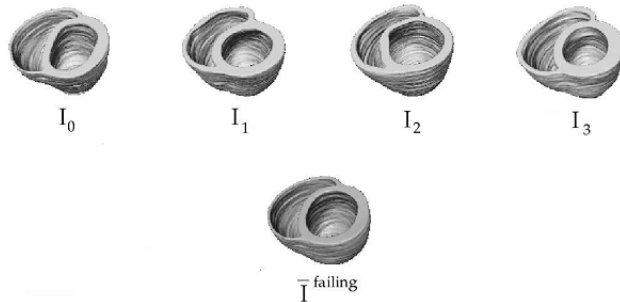


Figure 6: Segmented binary models of diseased dog hearts (I_0, I_1, I_2, I_3) used to compute \bar{I}^{failing} [4]

The conservation of momentum property and geodesic shooting described in section 3.4 has been used to extend LDDMM to build atlases. The use of geodesic shooting for computing atlases is as follows.

First, flows are generated from a template (picked arbitrarily as I_0) to each of the images. The average velocity vector fields are then computed from the initial vector fields of each flow as

$$\bar{v}_0 = \frac{1}{N} \sum_i v_0^i$$

Lastly, the averaged velocity field \bar{v}_0 is propagated forward via geodesic shooting with the same number of steps that was used to match each of the images with the template I_0 . The resulting flow is used to transform the template I_0 to generate the ensemble-averaged atlas. The process can be iterated with the newly generated average as the template I_0 and stopping when the averaged $\|\bar{v}_0\|$ reaches some small convergence tolerance.

This has been used to quantify variability in heart geometry[14].

4.2 Statistical Shape Analysis

LDDMM provides a linear setting for one to do statistics on inherently non-linear shape spaces. The underlying coordinate system Ω is the union of 0-D, 1-D, 2-D and 3-D manifolds. As described in section 3.4, the conservation

of momentum property parameterizes the entire flow by a single point in time at $t=0$. Thus doing statistical analysis on the velocity field $v(t)|_{t=0}$ or the momentum field $(L^\dagger L)v(t)|_{t=0}$ contains sufficient information about the entire flow.

A common analysis technique for multivariate data is Principle Component Analysis (PCA), also known as Karhunen-Loeve decomposition. This method builds a basis of the linear space that diagonalizes the covariance matrix. In doing so, it also orders the basis vectors in such a way that the first basis is along the direction with maximum variance and so on. For the uses of dimensionality reduction, it is sufficient to pick a value for L such that 95% of the variance is preserved

$$\sum_{i=1}^L \lambda_i \geq 0.95 \sum_{i=1}^M$$

The use of PCA in stochastic deformable models was popularized by Cootes[8]. Let

$$Y_{p \times N} = \{Lv^0, Lv^1, \dots, Lv^N\}$$

be the matrix of momentum fields with each momentum vector field a column vector. The number of rows equals the dimensionality of a momentum vector field, which equals $64 \times 112 \times 64 \times 3$ ¹ and the number of columns equals the number of subjects. Instead of the naive approach of computing the basis vectors of the covariance matrix resulting in matrices of enormous sizes, we compute the Singular Value Decomposition (SVD) of the original matrix $Y(x)$. The matrix Y can be factored via the SVD as

$$Y_{p \times N} = U_{p \times p} \Sigma_{p \times N} V_{N \times N}^T$$

and the following relations are equivalent

$$\begin{aligned} U^T Y &= \Sigma V^T \\ &= (V \Sigma^T)^T \end{aligned}$$

The eigenvectors of the covariance matrix K_Y are related to the column vectors of U upto a constant scaling factor and the eigenvalues of K_Y are the

¹this equals $1376256 \approx 1.37$ million rows

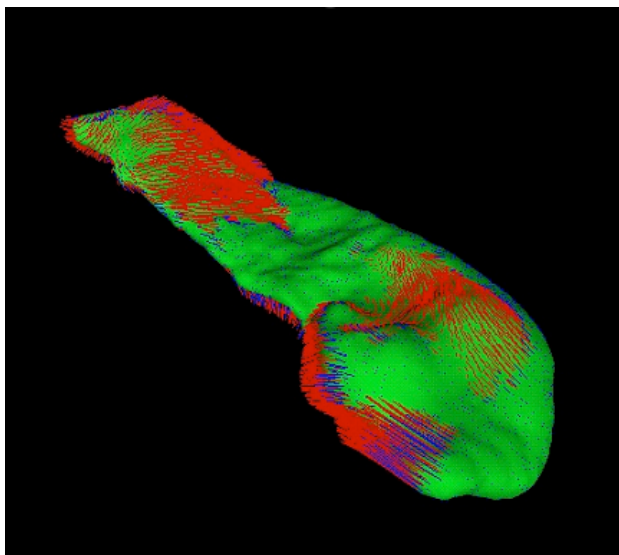


Figure 7: Hippocampus

squares of the singular values in Σ . From the SVD equation $Y = U\Sigma V^T$, we see that $YY^T = U\Sigma^2U^T$. Taking a subset L of the principle components, we have

$$U_L^T Y = \Sigma_L V_L^T = (V_L \Sigma_L^T)^T$$

Reconstructing the original data set with L principle components:

$$Y_L \approx U_L A_L$$

where $A_L = U_L^T Y$ is the matrix with the principle coefficients. These are the coordinates in the new basis.

4.3 Hippocampal Shape Discrimination

Rates of hippocampal volume loss have been shown to distinguish subjects with Dementia of the Alzheimer's Type (DAT) from controls with healthy aging[15]. Previous research in identifying differences in brain structures such as the hippocampus was done by analyzing the *displacement vector fields* between DAT and control subjects[10].

This section analyzes differences between DAT and control subjects by the use of the initial *momentum vector field*. Twenty-six subjects with Clinical Dementia Rating (CDR) 0 and eighteen subjects with CDR 0.5, for a total of forty-four subjects were recruited for the purposes of the study. An additional elder control subject (i.e., CDR 0) was used as a template (reference.) The left and right hippocampi were manually segmented out by a team of experts using previously described methods[13]. The left and right sides were then mapped from the template to each of the DAT and control subjects.

Previously an orthonormal basis was constructed on the displacement vector fields. This leads to diffeomorphic transformations only under the assumption of small deformations. When deformations are large, such as in cross-subject differences, the small deformation assumption breaks down. Thus, instead of performing PCA analysis on displacement fields under the L^2 metric, an analysis is performed with respect to the metric in space V used for generating the flow

$$\langle v, w \rangle_V = \langle Lv, Lw \rangle_{L^2} = \langle L^\dagger Lv, w \rangle_{L^2}$$

where $v, w \in V$, the Hilbert space of smooth velocity vector fields. As the initial momentum vector fields (i.e., $t = 0$) completely parameterizes the geodesic flow, we perform the PCA analysis on the quantity Lv_0 .

The construction is as follows. If

$$Y(x) = \{Lv^1(x), Lv^2(x), \dots, Lv^N(x)\}$$

is assumed to be a family of zero-mean Gaussian random vector fields with covariance structure

$$K_Y(x, y) = Y(x)Y(y)^T$$

then the set of orthogonal vectors that diagonalize the covariance matrix K_Y is the set of basis vectors $\{e_1(x), \dots, e_N(x)\}$ that maximize variance along each vector. This is the PCA. The basis vectors are constructed via the SVD as described in section 4.2. In this section, we follow the analysis as in [21], but only report the results on the left hippocampi.

The first twenty principle components and their coefficients, accounting for 82.9% of the total variance was used. Figure 8 shows the power law distribution of the full forty-four eigenvectors (there are as many eigenvectors

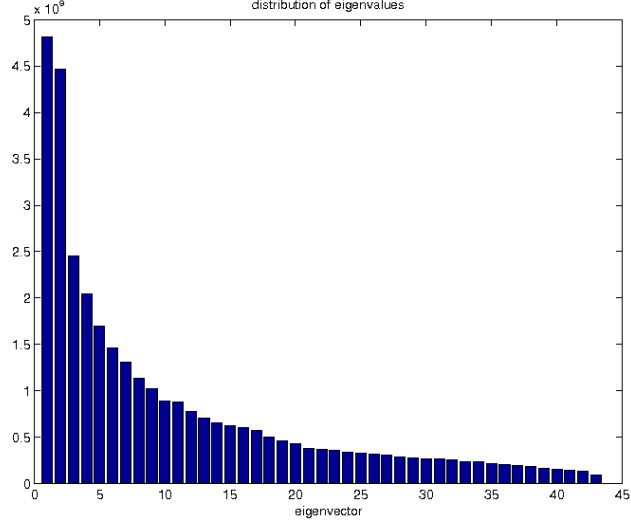


Figure 8: Eigenvalue distribution[21]

as there are subjects.) The first twenty principle components and their coefficients, accounting for 82.9% of the total variance was used. Once the dimensionality reduction was performed by means of discarding the unneeded eigenvectors, a non-parametric statistical test was conducted to check for group differences. To test the null hypothesis

$$\mathcal{H}_0 : \bar{Z}^{Ctrl} = \bar{Z}^{DAT} \quad (4.1)$$

we calculated the Hötelling's T^2 statistic for two samples as

$$T^2 = \frac{N_{Ctrl}N_{DAT}}{N_{Ctrl} + N_{DAT}} \times \left(\hat{Z}^{DAT} - \hat{Z}^{Ctrl} \right)^T \Sigma^{-1} \left(\hat{Z}^{Ctrl} - \hat{Z}^{DAT} \right)$$

Monte Carlo (MC) simulations were used to generate a large number of permutations. The collection of T^2 values from each permutation leads to an empirical $\hat{F}(\cdot)$ distribution according to

$$F_{M, N_{Ctrl} + N_{DAT} - M - 1} = \frac{N_{Ctrl} + N_{DAT} - M - 1}{(N_{Ctrl} + N_{DAT} - 2)M} T^2$$

The null hypothesis (equation 4.1) is rejected when the p-value

$$p = \int_{T^2}^{\infty} \hat{F}(f) df$$

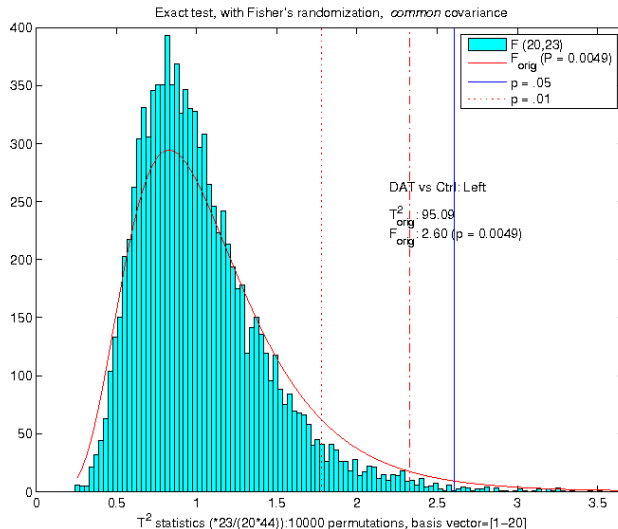


Figure 9: Empirical \hat{F} distribution from Hotelling's T^2 test with 10000 group permutations[21]

of the \hat{F} distribution falls below some predetermined significance value, usually 0.05. Figure 9 shows the results of the MC simulation. As the p-value is 0.0049, the null hypothesis that the two populations have the same means is rejected. Thus, it is worthwhile to do further analysis for classification on the left hippocampi.

5 Conclusion

The framework of CA introduces the concept of a deformable template being transformed by geodesic evolution equations under groups of diffeomorphisms. Specifically, the LDDMM algorithm introduces a metric space from the evolution equations along the geodesics connecting one anatomical object to another. The geodesic equations are derived using the Euler-Lagrange equations from the associated variational inexact matching problem. The initial momentum field enables a dimensionality reduction by parameterizing the whole geodesic flow at the initial time step. This has been used for the statistical shape analysis of the hippocampus in the dementia of the Alzheimer's type.

6 Acknowledgments

I would like to take this opportunity to express my gratitude to my supervisor, Dr. Faisal Beg. He not only patiently answered my numerous questions during our weekly meetings, but also pointed me towards additional literature. This section would not be complete without thanks to the members of Dr. Beg's group, specifically Ali Khan, Vinay Kotamraju, Sean Sutherland, Stephen Wong and Jingyun Chen who gave me a big hand in understanding LDDMM and the surrounding technologies. Ali also promised to buy me a drink if I cite his paper[4].

Glossary

L^2 -norm

norm of square integrable functions $\int_{\Omega} |\phi(x)|^2 dx$ 8

Computational Anatomy (CA)

the combination of biomedical imaging with computerized modeling to infer noninvasively the structural and functional properties of complex biological systems. 12, 17

Clinical Dementia Rating (CDR)

a numerical scale used to quantify the severity of symptoms of dementia. 14

Dementia of the Alzheimer's Type (DAT)

the development of multiple cognitive deficits; impairment of long-term and short-term memory. 14

Fast Fourier Transform (FFT)

an efficient algorithm of complexity $O(N \log N)$ to compute the discrete Fourier Transform and its inverse. 9

Hilbert space

a generalization of the vector algebra of Euclidean space to infinite dimensions. 9

Infimum inf

the greatest element of a set T that is less than or equal to all other elements of a subset S 9

Large Deformation Diffeomorphic Metric Mapping (LDDMM)

an algorithm to generate high resolution diffeomorphic mappings between anatomical images alongwith distances between them. 7, 8, 10, 12, 13, 17, 18

Monte Carlo (MC)

a nondeterministic numerical procedure to find solutions to mathematical problems like high dimensional integrals. [17](#)

Metric

a function that defines a distance between elements of a set. [9](#)

Magnetic Resonance Imaging (MRI)

a non-invasive imaging method that relies on the relaxational properties of excited hydrogen nuclei in water and lipids [1](#)

Principle Component Analysis (PCA)

a technique to reduce multidimensional data sets to lower dimensions for analysis [13](#), [15](#), [16](#)

Positron Emission Tomography (PET)

a non-invasive imaging method that relies on radioactive tracer isotopes decaying by emitting positrons [1](#)

Registration

the process of transforming different sets of data into one common coordinate system. [1](#)

Self-Adjoint operator

an operator \mathcal{A} that is equal to its adjoint \mathcal{A}^\dagger [9](#)

Sobolev norm

a norm that is a combination of L^p -norm as well as its derivatives.
 $\|f\|_p : \left(\int_D (|f|^p + |D_1 f|^p + \dots + |D_n f|^p) dv \right)^{1/p}$ [9](#)

Sobolev space

a vector space of functions equipped with a norm that is a combination of L^p -norm of the function itself as well as its derivatives upto a given order. [9](#)

Supremum sup

the least element of a partially ordered set T that is greater than or equal to each element of a subset S [9](#)

Singular Value Decomposition (SVD)

a generalization of the factorization of a square matrix into its eigenvalues and eigenvectors to non-square matrices [13](#), [14](#), [16](#)

References

- [1] Vladimir I. Arnold and Boris A. Khesin. *Topological methods in hydrodynamics*. Springer-Verlag New York, Inc., New York, NY, USA, 1998. 11
- [2] R.K. Bajcsy and S. Kovačič. Multiresolution elastic matching. 46(1):1–21, April 1989. 5
- [3] R. Barrett, M. Berry, T. F. Chan, J. Demmel, J. Donato, J. Dongarra, V. Eijkhout, R. Pozo, C. Romine, and H. Van der Vorst. *Templates for the Solution of Linear Systems: Building Blocks for Iterative Methods*. SIAM, Philadelphia, PA, 1994. 7
- [4] M.F. Beg and A. Khan. Computation of average atlas using LDDMM and geodesic shooting. *IEEE International Symposium on Biomedical Imaging: From Nano to Macro*, 6:1116 – 1119, 2006. 13, 19
- [5] M.F. Beg, M.I. Miller, A. Trouvé, and L. Younes. Computing large deformation metric mappings via geodesic flows of diffeomorphisms. *International Journal of Computer Vision*, 61(2):139–157, February 2005. 9
- [6] Y. Cao, M.I. Miller, R.L. Winslow, and L. Younes. Large deformation diffeomorphic metric mapping of vector fields. *IEEE Trans. Medical Imaging*, 24(9):1216–1230, September 2005. 3
- [7] G.E. Christensen, R.D. Rabbitt, and M.I. Miller. Deformable templates using large deformation kinematics. *IEEE Transactions on Image Processing*, 5(10):1435–1447, October 1996. 5, 6, 8
- [8] T.F. Cootes, C.J. Taylor, D.H. Cooper, and J. Graham. Active shape modelstheir training and application. *Computer Vision and Image Understanding*, 61:38 – 59, 1995. 14
- [9] T.F. Cootes, C.J. Twining, and C.J. Taylor. Diffeomorphic statistical shape models. pages xx–yy, 2004. 4
- [10] J. C. Csernansky, L. Wang, S. Joshi, J. Philip Miller, M. Gado, D. Kido, D. McKeel, J.C. Morris, and M.I. Miller. Early dat is distinguished from

- aging by high dimensional mapping of the hippocampus. *Neurology*, 55:1636–1643, 2000. [15](#)
- [11] P. Dupuis and U. Grenander. Variational problems on flows of diffeomorphisms for image matching. *Quarterly of Applied Mathematics*, 56:587–600, 1998. [9](#)
- [12] Jacques Hadamard. Sur les problèmes aux dérivés partielles et leur signification physique. *Princeton University Bulletin*, 13:49–52, 1902. [4](#)
- [13] J.W. Haller, A. Banerjee, G.E. Christensen, M. Gado, S. Joshi, M.I. Miller, Y. Sheline, M.W. Vannier, and J.G. Csernansky. Three-dimensional hippocampal mr morphometry with high-dimensional transformation of a neuroanatomic atlas. *Radiology*, 202:504–501, 1997. [16](#)
- [14] P. Helm, L. Younes, M.F. Beg, D. Ennis, C. Leclercq, O. Faris, E. McVeigh, M.I. Miller, and R. Winslow. Evidence of structural remodeling in the dyssynchronous failing heart. *Circulation Research*, pages 98–125, 2006. [13](#)
- [15] C.R.J. Jack, R.C. Petersen, Y. Xu, P.C. O’Brien, G.E. Smith, R.J. Ivnik, B.F. Boeve, E.G. Tangalos, and E. Kokmen. Rates of hippocampal atrophy correlate with change in clinical status in aging and ad. *Neurology*, 55:484–489, 2000. [15](#)
- [16] A.N. Kolmogorov and S.V. Fomin. *Introductory Real Analysis*. Dover, New York, 1970. [11](#)
- [17] M.I. Miller, G.E. Christensen, Y. Amit, and U. Grenander. Mathematical textbook of deformable neuroanatomies. 90(24), December 1993. [5](#)
- [18] M.I. Miller, A. Trounev, and L. Younes. Geodesic shooting for computational anatomy. *Journal of Mathematical Imaging and Vision*, 24(2):209–228, March 2006. [11](#), [12](#)
- [19] P.M. Thompson, R.P. Woods, M.S. Mega, and A.W. Toga. Mathematical/computational challenges in creating deformable and probabilistic atlases of the human brain. *Human Brain Mapping*, 9(2):81–92, 2000. [12](#)

- [20] Paul A. Viola. *Alignment by Maximization of Mutual Information*. PhD thesis, Massachusetts Institute of Technology, March 1995. [6](#)

- [21] L. Wang, M.F. Beg, T. Ratnanather, C. Ceritoglu, L. Younes, J.C. Morris, J.G. Csernansky, and M.I. Miller. Large deformation diffeomorphism and momentum based hippocampal shape discrimination in dementia of the alzheimer type. *IEEE Trans. Medical Imaging*, 26(4):462–470, April 2007. [16](#), [17](#), [18](#)